Sipos, T., and Merkel, J. R. (1970), *Biochemistry 9*, 2766.

Smith, R. L., and Shaw, E. (1969), *J. Biol. Chem. 244*, 4704.

Solomon, I. (1955), *Phys. Rev. 99*, 559.

Stroud, R. M., Kay, L. M., and Dickerson, R. E. (1971), *Cold Springs Harbor Symp. Quant. Biol. 36*, 125.

Stroud, R. M., Kay, L. M., and Dickerson, R. E. (1974), *J. Mol. Biol. 83*, 185.

Titani, K., Ericsson, L. H., Neurath, H., and Walsh, K. A. (1975), *Biochemistry 14*, 1358.

Trowbridge, C. G., Krehbiel, A., and Laskowski, M. (1963), *Biochemistry 2*, 843.

Valenzuela, P., and Bender, M. L. (1969), *Proc. Natl. Acad. Sci. U.S.A. 63*, 1214.

Valenzuela, P., and Bender, M. L. (1970), *Biochemistry 9*, 2440.

Van Geet, A. L., and Hume, D. N. (1965), *Anal. Chem. 37*, 979.

Villanueva, G. B., and Herskovits, T. T. (1971), *Biochemistry 10*, 4589.

Walsh, K., and Neurath, H. (1964), *Proc. Natl. Acad. Sci. U.S.A. 52*, 884.

Yguerabide, J., Epstein, H. F., and Stryer, L. (1970), *J. Mol. Biol. 51*, 573.

The Molecular Structure of a Dimer Composed of the Variable Portions of the Bence-Jones Protein REI Refined at 2.0-Å Resolution[†]

Otto Epp,* Eaton E. Lattman,‡ Marianne Schiffer,§ Robert Huber, and Walter Palm#

ABSTRACT: The structure of the variable portions of a κ-type Bence-Jones protein REI forming a dimer has been determined by X-ray diffraction to a resolution of 2.0 Å. The structure has been refined using a constrained crystallographic refinement procedure. The final R value is 0.24 for 15,000 significantly measured reflections; the estimated standard deviation of atomic positions is 0.09 Å. A more objective assessment of the error in the atomic positions is possible by comparing the two independently refined monomers. The mean deviation of main-chain atoms of the two chains in internal segments is 0.22 Å, of main-chain dihedral angles 6.3° for these segments. The unrefined molecular structure of the V_{REI} dimer has been published (Epp, O., Colman, P., Fehlhammer, H., Bode, W., Schiffer, M., Huber, R., and Palm, W. (1974), *Eur. J. Biochem. 45*, 513). Now a detailed analysis is presented in terms of hydrogen bonds and conformational angles. Secondary structural elements (antiparallel β structure, reverse turns) are defined. A more precise atomic arrangement of the amino acid residues forming the contact region and the hapten binding site is given as well as the localization of solvent molecules. Two *cis*-prolines (Pro-8 and Pro-95) were detected. The intrachain disulfide bridge (Cys-23–Cys-88) occurs statistically in two alternative conformations. The structure suggests reasons for strong conservation of several amino acid residues. The knowledge of the refined molecular structure enables crystal structure analyses of related molecules to be made by Patterson search techniques. The calculated phases based on the refined structure are much improved compared to isomorphous phases. Therefore the effects of hapten binding on the molecular structure can be analyzed by the difference Fourier technique with more reliability. Hapten binding studies have been started.

Immunoglobulins are proteins with specific antibody activity. There exist several classes. The IgG class of immunoglobulins is composed of two light and two heavy chains. The Bence-Jones proteins excreted by patients with multiple myeloma into the urine have been shown to be free light chains. The Bence-Jones protein REI is a human immunoglobulin light chain of κ type. The purification, crystallization, and sequence analysis has been described (Palm, 1970; Palm and Hilschmann, 1973, 1975; Palm, 1974). The crystal structure of a dimer composed of the variable portions of this Bence-Jones protein at a resolution of 2.8 Å was reported (Epp et al., 1974). Data to a resolution of 2.0 Å have now been collected and the structure has been refined by constrained crystallographic refinement. The aim was to get a detailed insight into the conformation of this molecule (main chain, side chains, and bound solvent) and to obtain a model sufficiently accurate for its use in Patterson search techniques to determine the crystal structures of related molecules (Fehlhammer et al., 1975). As refined phases are considerably better than isomorphous phases (Watenpaugh et al., 1973; Deisenhofer and Steigemann, 1975; Huber et al., 1974), the quality of difference Fourier maps will be much improved; this will make it possible to determine the structure bound haptens and the subtle structural changes

Table I: Options and Specifications of Various Programs.

(1) Model Building (Diamond, 1966)

Probe	Probe Length	Filter Constants				Variation of Dihedral Angles
		C_1		C_2		
1	1	0^a	0.5	1.0^a	10^{-4}	10^{-2a}	ϕ,ψ,χ
2	1	2	0.5	0.5	10^{-4}	10^{-4}	ϕ,ψ,χ,τ
3	2	5	0.1	0.1	10^{-4}	10^{-4}	ϕ,ψ,χ,τ
4	5	6	0.1	0.0	10^{-4}	10^{-2}	ϕ,ψ,χ,τ
5	6	6	0.0	0.0	10^{-4}	10^{-2}	ϕ,ψ,χ,τ

Eigenshifts are permitted if either $\lambda \geqslant C_1\epsilon^2$ or $\lambda \geqslant C_2\lambda_{max}$, where λ are eigenvalues of the normal matrix. ϵ^2 is the residual. Variation of the folds of prolines, χ^5 of arginine, and ω was not permitted. The angular value of τ ($N-C_\alpha-C$) was fixed to a value of $109.65°$ including model-building procedure 7. In model-building 7 cis-prolines were introduced (Huber and Steigemann, 1974). ϕ,ψ are main-chain dihedral angles, χ are side-chain dihedral angles. The angular values of main chain and side chains were used and included wherever they were known, even if only crudely.

(2) Real-Space Refinement (Diamond, 1971, 1974)

Zone length	7
Margin width	$6; 8^b$
Fixed radius of all atoms (Å)	$1.55; 1.50^c$
Relative weights of C:N:O:S	6:7:8:16
Relative softness of dihedral angles	
$\psi,\phi,\chi^1-\chi^4$	100
χ^5	1
$\theta^1,\theta^2,\theta^3$ (proline)	0.1
θ^1,θ^2 (cysteine)	0
τ ($N-C_\alpha-C$)	0.1
ω (torsion angle $C_{i-1}^\alpha-C_{i-1}-N_i-C_i^\alpha$)	0.1^d

Refinement of Scale Factor (K) and Background Level (d) Only

Filter ratio $\lambda_{min}/\lambda_{max}$ for K, d refinement	0.01
Filter ratio for rotational refinement $\lambda_{min}/\lambda_{max}$	
Isomorphous map	0.005
from difference Fourier map 2 on	0.0005
from difference Fourier map 4 on	0.00007
from difference Fourier map 6 on	0.00004
The value of 0.00004 resulted in a proportion of shifts applied of about	70%
Filter ratio for translational refinement $\lambda_{min}/\lambda_{max}$	0.01
The value of 0.01 resulted in a proportion of shifts applied of about	100%

(3) Structure—Factor Calculation

(W. Steigemann and T. A. Jones) atomic scattering factors: Forsyth and Wells constants (1959), an overall temperature factor was used throughout.

(4) R Value Calculation

R is defined as

$$R = \frac{\Sigma||F_o| - |F_c||}{\Sigma|F_o|}$$

$|F_o|$, observed structure—factor amplitude
$|F_c|$, calculated structure—factor amplitude
For this calculation, as well as for the Fourier calculations, reflections of extremely bad correlation were excluded. The condition for exclusion was:

$$\frac{2||F_o| - |F_c||}{||F_o| + |F_c||} > 1.2$$

About 250 reflections were excluded. The innermost reflections to 6.8-Å resolution were omitted from all calculations (941).

(5) Fourier Synthesis

Grid: 1.1 Å × 1.1 Å × 1.0 Å at the beginning to a resolution of 2.4 Å, later 0.8 Å × 0.8 Å × 0.8 Å. During the course of the refinement the Fourier coefficients were mostly of the type $(2|F_o| - |F_c|)$ $\exp\alpha_c$. Also some Fourier syntheses with coefficients $(3|F_o| - 2|F_c|)$ $\exp\alpha_c$ were used. Difference Fourier maps were calculated with coefficients $(|F_o| - |F_c|)$ $\exp\alpha_c \cdot \alpha_c$, calculated phase.

(6) Computer Time on a Siemens 4004/150 (Cycle Time 0.75 μsec)

Structure—factor calculation for 15,000 reflections and 1630 atoms	13,500 sec
Fourier synthesis 1.62×10^5 grid points	4000 sec
Real-space refinement for both chains in the asymmetric unit	17,000 sec

^{a}These values were used in model-building procedures 8 and 9 for probe length and filter constants. Also the variation of the angular value of τ was allowed, but not for Gly, Ser, and Thr. ^{b} After introduction of ω. ^{c}New value estimated with the data at 2.1-Å resolution. $^d\omega$ has been introduced after difference Fourier map 4 (data to 2.3-Å resolution, R factor value 0.29, B = 23 Å^2).

Experimental Procedure

The V_{REI} dimer crystallizes in the space group $P6_1$. The hexagonal unit cell parameters are $a = b = 75.8$ Å, $c = 98.2$ Å, $\gamma = 120°$. The asymmetric unit contains one dimer molecule. Intensity data were collected to 2.0-Å resolution on a modified Siemens AED diffractometer using $\theta-2\theta$ scan, with focus-to-crystal and crystal-to-detector distances of 30 cm each. The intensity profile of each reflection was scanned twice in steps of $1/100°$ (44 steps over the whole reflection). The counting time per step was set inversely proportional to the intensity at the peak of the reflection; the upper limit was set at 2.4 sec/step for reflections to a resolution of 2.5 Å. The reflections from 2.5- to 2.0-Å resolution were measured with 6 sec/step. Background was counted on both sides. The whole data set had been collected by diffractometers. The reflections were collected in shells of $\sin\theta/\lambda$. Film data obtained from screenless preces-

Schwager et al. (Schwager et al., 1975) were included and used for scaling purposes. The data were corrected for absorption by an empirical method (Huber and Kopfmann, 1969). The complete intensity data set included 42,464 measurements (of which 5454 are film data), which were merged to 14,993 independent reflections (0.69 of the possible reflections to a resolution of 2.0 Å). All reflections to a resolution of 2.5 Å were used (10381), except the innermost reflections to a resolution of 6.8 Å (941) which are strongly influenced by the solvent continuum. To a resolution of 2.5 Å, 0.99 of the possible reflections is measured. From 2.5- to 2.0-Å resolution, only the reflections which could be observed above the 2σ significance level determined from counting statistics (3671) were used (e.g., 0.34 of the possible reflections in that range).

The neglect of the innermost reflections to a resolution of 6.8 Å does not influence Diamond's real-space refinement

Steigemann, 1975) the neglect of the innermost reflections improved the refinement of the positions of solvent molecules. We omitted these reflections from all calculations and did not consider them in the interpretation of the electron density map. The R value for all measurements, defined as

$$R = \left(\sum_h \sum_j^{N_h} (\langle I \rangle_h - I_{hj})^2 \Big/ \sum_h N_h \langle I \rangle_h^2 \right)^{1/2}$$

is 0.05 ($\langle I \rangle_h$ is the average intensity of the N_h measurements, I_{hj} are the individual measurements of a reflection h). The R_{sym} values for individual crystals lie between 0.022 and 0.065; the average R_{sym} is 0.04.

The crystal structure of REI has been refined by a constrained crystallographic refinement described in the refinement of the crystal structure of the bovine pancreatic trypsin inhibitor (PTI) (Deisenhofer and Steigemann, 1975) and in the refinement of the structure of the complex between bovine trypsin and PTI (Huber et al., 1974). This procedure involves cycles consisting of phase calculation using the current atomic model, Fourier synthesis using these calculated phases and the observed structure-factor amplitudes, and Diamond's real-space refinement (Diamond, 1971, 1974). At various stages (stagnation of further refinement), difference Fourier syntheses are calculated to detect and correct gross errors in the model (such as incorrect orientation of main-chain amides or side chains) and to localize solvent molecules. The stagnation of the refinement is reached, if the R factor value (definition see Table I) does not decrease further. Incorrectly oriented main-chain amides are rotated by reading the correct position of the carbonyl oxygen from the difference map and subjecting the whole chain to a model-building procedure (Diamond, 1966). Side-chain orientations are corrected by rotating around the appropriate dihedral angles. Some characteristics of the model-building procedure and the real-space refinement procedure are outlined in Table I. During the refinement 8 model-building procedures and 11 difference Fourier syntheses were calculated. The Fourier syntheses in the automatic cycles between these difference Fourier maps were mostly of the type $(2|F_o| - |F_c|)$ exp α_c; a few $(3|F_o| - 2|F_c|)$ exp α_c were also used. Such syntheses increase the density gradients at the atomic positions and the speed of convergence. Table II shows the statistics of the course of the real-space refinement procedure.

Results and Discussion

Description of the Refinement. The starting model had been obtained through extensive real-space refinement of the model into the isomorphous Fourier map at 2.8-Å resolution. The above electron density map had first been averaged over the two independent molecules (Epp et al., 1974). The starting R factor (defined in Table I, 4) was 0.48. During the subsequent course of the refinement the two molecules in the asymmetric unit were refined independently. The coordinates of the second molecule were obtained by applying the known local symmetry. After several cycles the R factor decreased to a value of 0.39. At this stage, the first difference Fourier map was calculated. The coordinates were plotted onto the Fourier map to check the progress. Misplaced side chains and several incorrectly oriented main-chain amides were detected (Table II). Between succeeding difference Fourier maps three to five automatic refinement cycles were performed, depending on the progress

Table II: Specifications of Difference Fourier Maps.

Difference Map No.	R Value	Corrections in Each Map Side Chains Main-Chain Amides Chain 1	Chain 2	Resolution (Å)	Overall Temp Fact. (Å²)	Atom Radius $\langle r \rangle$ (Å)
1	0.390	10	7	2.5	28	1.55
2	0.350	4	6	2.4	25	1.55
3	0.304	3	2	2.4	23	1.55
		11 solvent molecules				
4	0.294	4	2	2.3	23	1.55
		26 solvent molecules				
5	0.282	4	3	2.3	23	1.55
		40 solvent molecules				
6	0.270	1	1	2.2	23	1.55
		39 solvent molecules introduction of cis-prolines (Pro-8, Pro-95)				
7	0.264	1	1	2.2	23	1.55
		42 solvent molecules				
8	0.250	1	1	2.2	23	1.55
		36 solvent molecules				
9	0.241			2.1	23	1.55
		41 solvent molecules				
10	0.241			2.1	23	1.50
		55 solvent molecules				
11	0.241			2.0	21	1.50
		53 solvent molecules				

tion data to 2.5-Å resolution. During the course of the refinement further data were included to 2.0-Å resolution. An overall temperature factor was used, which was recalculated several times by comparing $|F_o|$ and $|F_c|$ and the temperature factor changed if necessary. An average atomic radius of 1.55 Å was used for all atoms throughout the refinement until difference Fourier map 9. Afterwards a new value of 1.50 Å was estimated by a trial calculation of atomic radii refinement in the real-space refinement step. This value is directly related to and consistent with the observed overall temperature factor of 21 Å². By the inspection of the difference Fourier maps, solvent molecules were detected and used in the phase calculations. The course of the difference maps is shown in Table II. The starting model had to be corrected in several segments. A number of main-chain amides and side chains had to be rotated. For the correction of main-chain amides, the presence of two identical molecules in the asymmetric unit provided a very useful cross-check. In difference Fourier map 6, the segments around Pro-8 and Pro-95 could be corrected. The local distribution of maxima and minima in these two regions was very similar and consistent in the two independent molecules, and it suggested the presence of cis-peptide groups (Huber and Steigemann, 1974). After the introduction of these *cis*-prolines, the refinement proceeded and stopped finally at an R factor value of 0.24. At this stage, 53 solvent molecules had been identified.

Description of the Electron Density Map. Figure 1a and b is stereo pictures of the electron density and the model fit at two amino acid residues (Gln-37 and Tyr-71)[1] in order to

[1] Amino acid residue numbers are those of the V_{REI} sequence. The nomenclature recommended by IUPAC-IUB (1970) is used in this paper with additional definitions as given by Diamond (1966, 1971, 1974). The coordinates of the V_{REI} dimer are available upon request. They are also in the Protein Data Bank of Brookhaven National Laboratory. Coordinates as well as stereo drawings are contained in R.
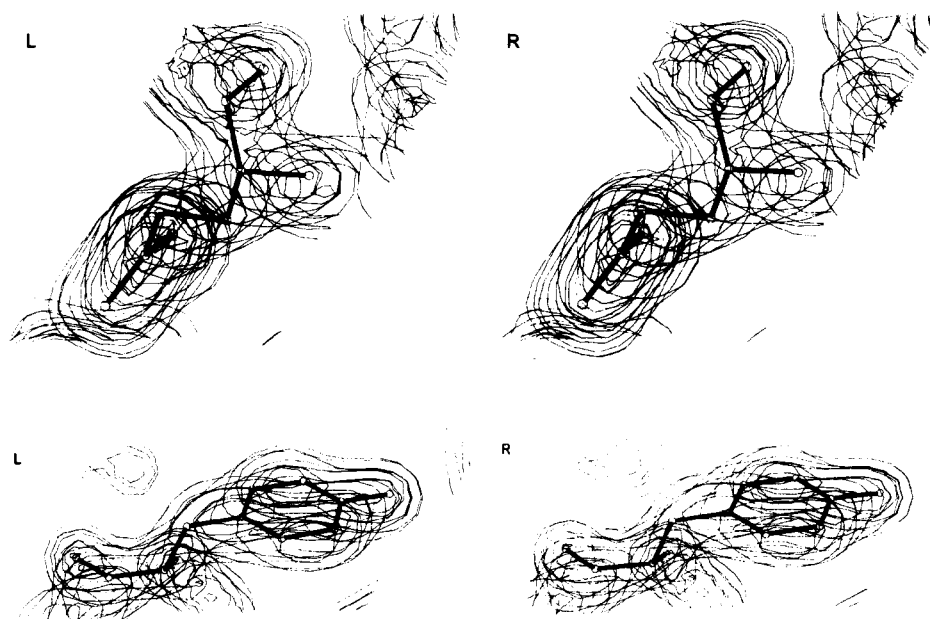
FIGURE 1: Electron density and model fit at two amino acid residues (top, Gln-37; bottom, Tyr-71). Contours in these figures from 0.3 e/Å^3 in steps of 0.3 e/Å^3.

demonstrate the quality of the final Fourier map. A typical electron density for carbon is 0.8 e/Å^3 and for oxygen 0.9 e/Å^3.

The final difference Fourier map is clear and suggests that the molecular structure is correctly interpreted. There is still some positive and negative residual density. Because of the restricted rotations about the S–S bond, cystine can exist in two mirror-image forms (Beychok, 1967). In the $V_{REI}{}^2$ monomer there is one intrachain disulfide bridge (Cys-23–Cys-88). Both conformations, differing predominantly in the position of 23 S$^\gamma$, occur statistically in about the same proportion in each monomer. This is shown in Figure 2a and b where sections 27–34 of difference Fourier maps ($F_o - F_c$) based on both conformations are drawn for monomer 2. Figure 2a shows the final difference map.

Figure 2b shows a difference map based on the alternative cystine conformation in the molecule. The difference between the two configurations is essentially expressed in the value of the side-chain dihedral angle χ^3 (rotation about the S–S bond). It differs by 162°. The final difference Fourier map also shows two statistical positions for the side chain of Gln-100.

Besides these there are about 40 negative peaks with height −0.20 e/Å^3, 20 with height −0.25 e/Å^3, and a few with height −0.30 e/Å^3. About 15 residual density peaks are positive, the highest is +0.25 e/Å^3. The positive peaks are near atomic positions, the negative features occur mainly at carbonyl oxygens, at the badly defined region of the N-terminus, at Gly-41, and at C$^\epsilon$ and N$^\zeta$ of lysine side chains. The negative residual density at carbonyl oxygens has also been observed in the PTI-trypsin complex and suggests that main-chain vibration affects predominantly

the carbonyl oxygens. Six of the 53 water molecules found at the end of the refinement, and included in the calculations with full occupancy and a temperature factor of 21 Å^2, lie in negative density of −0.25 e/Å^3.

Accuracy of the Structure; Comparison of the Two Monomers. A comparison of the dihedral angles of the two main chains shows that only at the N- and C-termini, which are badly defined, at some Gly residues (Gly-57, Gly-64), and in some external loops (12–18, 26–34 first hypervariable region, 40–44, 78–81, 93–97 part of the third hypervariable region) the differences between the two chains are considerably larger than the mean deviation $\langle \Delta\phi,\psi \rangle$ of 9.6°. There are particularly large discrepancies in ϕ and ψ at Ser-26, Gln-27, and Asp-28. We observed no significant deviation in dihedral angles of residues forming the monomer–monomer contact across the local diad (see Figure 5). The segments deviating significantly from the local symmetry face the solvent, and the reasons for these structural differences are unclear. As the difference map is featureless in these regions (Gln-27 is visible only to C$^\gamma$ in both chains) these structures appear to represent real alternative conformations. The mean deviation excluding these segments is $\langle \Delta\phi,\psi \rangle$: 6.3°. The same result is reflected by a comparison of the main-chain atoms (N, C$^\alpha$, C$^\beta$, C, O) of internal segments of both monomers (segments 4–10, 19–25, 35–38, 45–49, 62–77, 84–89, and 97–102). The mean deviation $\langle r \rangle$ is 0.22 Å compared with 0.47 Å for all atoms (the mean deviation of the internal segments for PTI and PTI complexed with trypsin is 0.25 Å, Huber et al., 1974). The average shift of main-chain atoms from the starting model (identical monomers) to the final model was 0.79 Å neglecting N- and C-terminal segments. A comparison of side-chain dihedral angles shows larger differences, especially at residues Ser, Thr, Gln, and Lys.

An objective assessment of the error of 0.2 Å, in the atomic coordinates of the final model, is possible by comparing the two chains forming the dimer. This estimate is

---

^{2} Abbreviations used are: F$_{ab}$', antigen-binding fragment of immunoglobulins; V$_{REI}$, variable part of the Bence-Jones protein REI; V$_L$, variable part of light chain; L1, L2, and L3 are the first, second, and *third hypervariable regions of light chains*; κ, λ, the two major types of light chains differentiated by their C-terminal amino acid sequences;
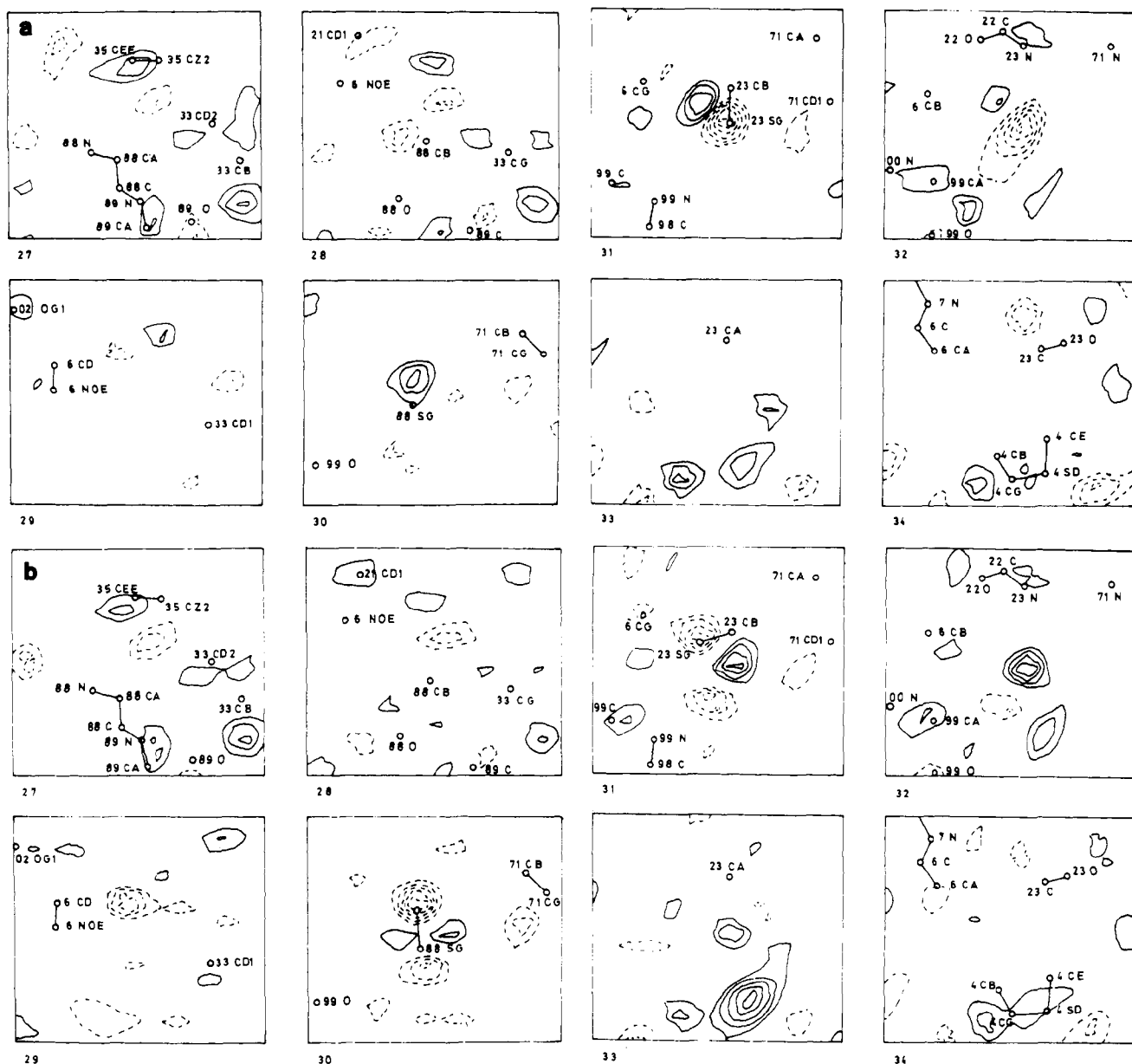
FIGURE 2: Sections 27–34 of difference Fourier maps ($F_o - F_c$) based on one of both possible cystine (Cys-23–Cys-88) conformations, respectively (shown is monomer 2). Contours from 0.10 e/Å³ in steps of 0.05 e/Å³: (—) positive, (- - -) negative residual densities. (a) Final difference map; (b) an intermediate state of the refinement. This explains the high residual density below Met-4 SD.

ations on dimer formation.

An estimate of the accuracy of the final atomic positions can also be deduced by Cruickshank's formulas using the residual and the curvature of the electron density at the atomic positions (Cruickshank, 1949). The mean height of carbonyl oxygens in the final Fourier map is 0.9 e/Å³. This yields a curvature of −1.32 e/Å⁵ (Stout and Jensen, 1968; Watenpaugh et al., 1973). The resulting standard deviation is $\sigma(x) = 0.09$ Å. This is comparable to the values obtained for PTI–trypsin complex (Huber et al., 1974).

Description of the Monomer. The V_{REI} monomer has a sandwich-like structure. The polypeptide chain can be divided into nine segments, which form two halves partly consisting of anti-parallel β structure. These segments are connected by reverse turns. The two sheets cover a hydrophobic interior containing several invariant or almost completely conserved amino acid residues in κ-light chains (Epp et al.,

part of three strands. The N-terminal strand adds to the upper sheet in a parallel and to the lower sheet in an antiparallel fashion. The lower part is a rather regular anti-parallel β-pleated sheet. An analysis of the conformational angles of the participating amino acid residues (5–7, 19–24, 63–65, and 71–75) yields mean values for ϕ and ψ of −117 and +140°, respectively, with standard deviations of 15 and 16°.

The ϕ and ψ values for a regular anti-parallel β structure (β-poly(L-alanine)) are −139 and +135° (Arnott et al., 1967). The remaining residues of the lower molecular part are involved in reverse turns. In the upper part, a regular antiparallel β-structure conformation is formed by two strands containing the residues 34–38 and 85–89. The analysis of the conformational angles yields mean values for ϕ and ψ of −116 and +137° with standard deviations of 13 and 11°, respectively. The other three strands of that mo-

DOCKET ALARM

Explore Litigation Insights

Docket Alarm provides insights to develop a more informed litigation strategy and the peace of mind of knowing you're on top of things.

Real-Time Litigation Alerts

Keep your litigation team up-to-date with **real-time alerts** and advanced team management tools built for the enterprise, all while greatly reducing PACER spend.

Our comprehensive service means we can handle Federal, State, and Administrative courts across the country.

Advanced Docket Research

With over 230 million records, Docket Alarm's cloud-native docket research platform finds what other services can't. Coverage includes Federal, State, plus PTAB, TTAB, ITC and NLRB decisions, all in one place.

Identify arguments that have been successful in the past with full text, pinpoint searching. Link to case law cited within any court document via Fastcase.

Analytics At Your Fingertips

Learn what happened the last time a particular judge, opposing counsel or company faced cases similar to yours.

Advanced out-of-the-box PTAB and TTAB analytics are always at your fingertips.

API

Docket Alarm offers a powerful API (application programming interface) to developers that want to integrate case filings into their apps.

LAW FIRMS

Build custom dashboards for your attorneys and clients with live data direct from the court.

Automate many repetitive legal tasks like conflict checks, document management, and marketing.

FINANCIAL INSTITUTIONS

Litigation and bankruptcy checks for companies and debtors.

E-DISCOVERY AND LEGAL VENDORS

Sync your system to PACER to automate legal marketing.

fastcase®
Smarter legal research.